Fuel 132 (2014) 135–148

Contents lists available at ScienceDirect

Fuel

journal homepage: www.elsevier.com/locate/fuel

An investigation of diesel–ignited propane dual fuel combustion in a heavy-duty diesel engine

Andrew C. Polk, Chad D. Carpenter, Kalyan Kumar Srinivasan, Sundar Rajan Krishnan *

Department of Mechanical Engineering, Mississippi State University, MS 39762, USA

HIGHLIGHTS

- Diesel–propane dual fuel combustion studied on a modern heavy-duty diesel engine (HDDE).
- Limitations to maximum achievable propane substitutions identified over a range of BMEPs (5–20 bar).
- Systematic analysis of combustion heat release, efficiencies, NO_x, smoke, HC, CO emissions.
- One of the first studies of exhaust particle size distributions with diesel–propane combustion in HDDE.
- Fueling strategy and diesel injection timing studies performed at 10 bar BMEP.

ARTICLE INFO

Article history:
Received 15 December 2013
Received in revised form 15 April 2014
Accepted 18 April 2014
Available online 6 May 2014

Keywords:
Dual fuel combustion
Propane
Particle size
Pilot ignition
NO_x emissions

ABSTRACT

This paper presents a detailed experimental analysis of diesel–ignited propane dual fuel combustion on a 12.9-l, six-cylinder, production heavy-duty diesel engine. Gaseous propane was fumigated upstream of the turbocharger air inlet and ignited using direct injection of diesel sprays. Results are presented for brake mean effective pressures (BMEP) from 5 to 20 bar and different percent energy substituted (PES) by propane at a constant engine speed of 1500 rpm. The effect of propane PES on apparent heat release rates, combustion phasing and duration, fuel conversion and combustion efficiencies, and engine-out emissions of oxides of nitrogen (NO_x), smoke, carbon monoxide (CO), and total unburned hydrocarbons (HC) were investigated. Exhaust particle number concentrations and size distributions were also quantified for diesel–ignited propane combustion. With stock engine parameters, the maximum propane PES was limited to 86%, 60%, 33%, and 25% at 5, 10, 15, and 20 bar BMEPs, respectively, either by high maximum pressure rise rates (MPRR) or by excessive HC and CO emissions. With increasing PES, while fuel conversion efficiencies increased slightly at high BMEPs or decreased at low BMEPs, combustion efficiencies uniformly decreased. Also, with increasing PES, NO_x and smoke emissions were generally decreased but these reductions were accompanied by higher HC and CO emissions. Exhaust particle number concentrations decreased with increasing PES at low loads but showed the opposite trends at higher loads. At 10 bar BMEP, by adopting a different fueling strategy, the maximum possible propane PES was extended to 80%. Finally, a limited diesel injection timing study was performed to identify the optimal operating conditions for the best efficiency-emissions-MPRR tradeoffs.

Abbreviations: AHRR, apparent heat release rate (gross); ATDC, after TDC; BDC, bottom dead center; BMEP, brake mean effective pressure; NO_x, brake-specific oxides of nitrogen; CA10-90, crank angle duration between 10% and 90% of cumulative heat release; CA5, crank angle at which 5% of cumulative heat release occurs; CA50, crank angle at which 50% of cumulative heat release occurs; CAD, crank angle degrees; CO, carbon monoxide; dB, decibels; DATDC, degrees after TDC; DBTDC, degrees before TDC; DCAT, Drivven combustion analysis toolkit; D_p, particle diameter; ECU, engine control unit; EEPS, engine exhaust particle sizer; EGR, exhaust gas recirculation; EUP, electronic unit pump; FCE, fuel conversion efficiency (brake); FID, flame ionization detector; FSN, filter smoke number; HC, total unburned hydrocarbons; ID_A, apparent ignition delay; IMEP, indicated mean effective pressure; LFE, laminar flow element; LHV, lower heating value; MPRR, maximum pressure rise rate; PES, percent energy substitution (by propane); PM, particulate matter; SOC, start of combustion; SOI, start of injection (commanded) of pilot fuel; TDC, top dead center; VNT, variable nozzle turbocharger.

* Corresponding author. Address: Department of Mechanical Engineering, Mississippi State University, 210, Carpenter Building, Mississippi State, MS 39762, USA. Tel.: +1 662 325 1544; fax: +1 662 325 7223.

E-mail address: krishnan@me.msstate.edu (S.R. Krishnan).

http://dx.doi.org/10.1016/j.fuel.2014.04.069
0016-2361/

1. Introduction

Despite their high fuel conversion efficiencies, conventional diesel engines suffer from high engine-out particulate matter (PM) and oxides of nitrogen (NO_x) emissions. Current (2010) US EPA emissions standards dictate that heavy duty diesel engines should comply with PM and NO_x limits of 0.013 g/kWh and 0.268 g/kWh, respectively [1]. In addition, intense energy sustainability debates have provided the impetus to investigate alternatives to liquid fossil fuels. In this regard, dual fuel combustion has received renewed interest due to its adaptability for alternative fuels and due to selected performance and emissions benefits compared to conventional diesel combustion [2]. Dual fuel combustion [3–5] is an approach that utilizes a high-cetane (easy-to-autoignite) "pilot" fuel such as diesel [5], biodiesel [6–8], or dimethyl ether [9] to ignite a low-cetane (difficult-to-autoignite) "primary" fuel. While gaseous low-cetane fuels such as natural gas, biogas, hydrogen, etc., have also been considered for dual fuel combustion [10–17], propane is a relatively more attractive option in the United States due to the existing widespread propane distribution network and the ease of storage and transportation of propane in the liquid phase at typical pressures of 100–200 psig (700–1400 kPa). In this regard, some previous studies [18–22] have examined the performance, emissions, and combustion characteristics of diesel–ignited propane (diesel–LPG) dual fuel combustion in both heavy-duty and light-duty diesel engines.

Under certain engine operating conditions, dual fuel combustion can provide superior engine performance and lower NO_x and PM emissions compared to straight diesel combustion. In conventional direct injection diesel combustion [23], NO_x is formed in the high-temperature diffusion flame surrounding the diesel jet while PM is formed in fuel-rich premixed regions (equivalence ratios (Φ) from 2 to 4) throughout the cross section of the diesel jet (especially in the head vortex region). In general, both NO_x and PM emissions from conventional DI diesel combustion can be attributed to high-temperature regions with rich-to-stoichiometric equivalence ratios. However, most strategies for NO_x reduction (e.g., exhaust gas recirculation, EGR) result in higher PM emissions and vice versa, leading to the well-known NO_x-PM tradeoff in conventional diesel combustion. By comparison, with dual fuel combustion, NO_x and PM emissions can be simultaneously reduced by increasing the substitution of the low-cetane fuel, which decreases the size of the high-temperature fuel-rich regions. For example, in conventional dual fuel combustion, the low-cetane fuel is inducted with the intake air forming a lean fuel–air mixture and is ignited by the timed injection of the high cetane fuel near TDC [5]. Since a large portion of the fuel energy arises from combustion of the lean fuel–air mixture, there are fewer locally rich areas, which reduce PM formation [5]. Further, as the low-cetane fuel substitution is increased at a constant load, the diesel fueling rate is reduced. Therefore, smaller diesel sprays result in fewer local high-temperature regions, thereby reducing NO_x emissions [5]. While PM mass emissions are reduced as the low-cetane fuel substitution is increased in dual fuel combustion, some studies on premixed charge compression ignition combustion [24,25] indicate that a reduction in PM mass may also be accompanied by an increase in particle number emissions. More recently, Zhou et al. [26] investigated the particle number emissions and particle size distributions in a micro-diesel pilot-ignited natural gas engine and concluded that both pilot injection timing and pilot diesel mass affect the particle number emissions with larger pilot masses leading to higher particle mass concentrations and lower particle number concentrations.

The NO_x and PM benefits possible with dual fuel combustion are partially offset by higher carbon monoxide (CO) and total unburned hydrocarbon (HC) emissions, resulting from partial oxidation and bulk quenching, respectively [5]. In addition, depending on the type of low-cetane fuel used, dual fuel combustion is often constrained by high pressure rise rates and the incidence of knock at high loads [27] and engine combustion instability leading to partial misfire at low loads [28].

Karim [5] described three stages of normal dual fuel combustion: (1) ignition of the high-cetane pilot fuel, (2) ignition of the fuel–air mixture near the pilot fuel spray, and (3) combustion of the remainder of the primary fuel–air mixture by flame propagation. The ignition delay period and the ensuing combustion processes are affected by the percent energy substituted (PES) by the low-cetane primary fuel (i.e., primary fuel concentration in the cylinder charger) as well as the type of primary fuel used [29]. For example, propane substitution has been shown to decrease ignition delay at high engine loads, while methane substitution only increases the ignition delay [30,31]. In addition, Liu and Karim [32] demonstrated that the most important factors affecting the ignition delay period in dual fuel engines include in-cylinder pressure and temperature histories (that are affected by the PES of the gaseous fuel), pre-ignition energy release, heat transfer to the cylinder walls, and residual gas fraction inside the cylinder. While many studies have examined dual fuel combustion on single-cylinder research engines or multi-cylinder light-duty engines (e.g., [18,22]), only a few researchers (e.g., [19]) have reported diesel–ignited propane combustion results from heavy-duty engines. The present work is an attempt to characterize diesel–ignited propane dual fuel combustion, performance, and emissions over a range of engine loads on a modern heavy-duty diesel engine.

2. Objectives

The objectives of this paper are listed below:

1. To investigate the effect of propane substitution on diesel–ignited propane dual fuel combustion on a heavy-duty diesel engine at different loads and the maximum torque speed with stock engine control parameters.
2. To characterize diesel–ignited propane dual fuel combustion based on cylinder pressure and heat release data, fuel conversion and combustion efficiency measurements, and gaseous and particle emissions results.

3. Experimental setup

The experiments were performed on a heavy-duty six-cylinder turbocharged direct-injection diesel engine, whose details are provided in Table 1. As shown in the schematic of the experimental setup (Fig. 1), the engine was coupled to a Froude Hofmann AG500 (500 kW) dynamometer. Two independent controllers were available for the engine: the stock engine control unit (ECU) and a LabVIEW-based, open-architecture Drivven engine controller. Flexible control of all engine parameters was possible using the Drivven engine controller. The stock ECU was used for most of the experiments reported here, except the final set of experiments that were performed to improve propane substitution and to investigate different injection timings at 10 bar brake mean effective pressure (BMEP). A custom-built ECU harness adapter board was used to enable a seamless transition from using the stock ECU to control the engine to the Drivven controller.

3.1. Steady state data acquisition

Steady state data acquisition included measurements of fuel and air mass flow rates, and temperatures and pressures at various

Table 1
Heavy-duty engine specifications.

Engine type	Six-cylinder, 4-stroke
Bore × Stroke × Connecting Rod Length	130 mm × 162 mm × 262 mm
Displacement	12.9 l
Compression ratio	17:1
Valves per cylinder	4
Fuel injection system	Solenoid direct injection with electronic unit pumps (EUPs)
Injection timing	Variable
Aspiration	Variable nozzle turbocharger (VNT)
EGR	Cooled

locations on the engine. The pilot diesel flow rate was measured with an Emerson Micro Motion coriolis mass flow meter (Model: CMF025M319N2BAEZZZ with an accuracy of 0.05% of reading). To facilitate accurate fuel measurement with one flow meter and to allow diesel to return from the engine simultaneously, a diesel level tank (Application Engineering, Inc.) was used. The level tank functions by regulating flow from the flowmeter using a float device. As diesel exits the system and is consumed in the engine, more diesel is supplied to the level tank at the same rate by an Airdog Class 8 Fuel Preparator pump/filter combination unit, which removes gaseous bubbles and water from the diesel in addition to solid contaminants. A bypass-style fuel pressure regulator was used to regulate diesel pressure at the inlet of the level tank to a maximum of 6 psig. The diesel fuel was conditioned using a shell-and-tube heat exchanger, a three-way mixing valve, and a temperature controller. Intake air mass flow rate was measured with a Meriam Laminar Flow Element (LFE Model: MC2-6) combined with an Omega Model MM custom differential pressure transducer. Straight intake piping (6-in. diameter) with lengths of ten pipe diameters upstream and five pipe diameters downstream of the LFE were used to facilitate laminar intake air flow. The gaseous propane mass flow rate was also measured with an Emerson Micro Motion coriolis flowmeter (Model: CMF025M319N2BAEZZZ with an accuracy of 0.35% of reading). Engine coolant, dynamometer, post-intercooler, intake mixture (after EGR mixing), fuel, and post-turbo exhaust temperatures were measured with Type K thermocouples. Pressures in the test cell were measured with Omega MM Series custom pressure transducers. The absolute pressure transducer (for the LFE flow) had a range of 0–30 psia (0.08% full-scale best straight line (FS BSL) accuracy), the differential pressure transducer for LFE flow had a range of 0–10 inches of H_2O (0.03% FS BSL), and the remaining gauge pressure transducers (for boost, exhaust, fuel, coolant, propane, and oil) had ranges of either 0–50 psig or 0–150 psig (0.25% FS BSL). Propane was fumigated into the intake air stream at the turbocharger inlet and directed downstream. Propane flow rate was varied by a manually controlled needle valve. A pressure regulator and a solenoid valve (for emergency shutoff) were utilized for propane operation up to 50 psig and placed upstream of the needle valve. Liquefied propane was stored in three 100 lbm propane cylinders connected in parallel. Each cylinder was equipped with a high pressure regulator (up to 150 psig) and a flash arrestor. Propane supply pressures were regulated to a sufficiently low pressure with the pressure regulator to ensure that all of the propane that entered the coriolis flow meter was always in the vapor phase at room temperature.

All exhaust emissions were measured downstream of the turbocharger turbine. Gaseous emissions were measured with an exhaust emissions bench (EGAS 2M) manufactured by Altech Environnement S.A. and smoke (expressed as Filter Smoke Number or FSN) was measured with an AVL 415S variable sampling smoke meter. The EGAS 2M bench allowed measurements of total HC emissions with a heated flame ionization detector (FID), NO_x emissions with a chemiluminescence detector, carbon dioxide in the exhaust and intake mixture (CO_2, CO_2-EGR) and CO emissions with a non-dispersive infrared analyzer, and oxygen (O_2) with a paramagnetic detector. Particle number concentrations and size distributions in the exhaust stream were measured with a TSI Engine Exhaust Particle Sizer (EEPS). Exhaust emissions were sampled with a rotating disk thermo-dilutor (TSI Model 3090) with a dilution factor of 1:261 and then passed through the EEPS. An AVL SESAM i60 FT Fourier Transform Infrared (FTIR) analyzer was available for more detailed speciation of gaseous exhaust emissions but these data were not obtained in the present experiments.

Data were collected and post-processed using National Instruments PXI hardware and the Drivven Combustion Analysis Toolkit

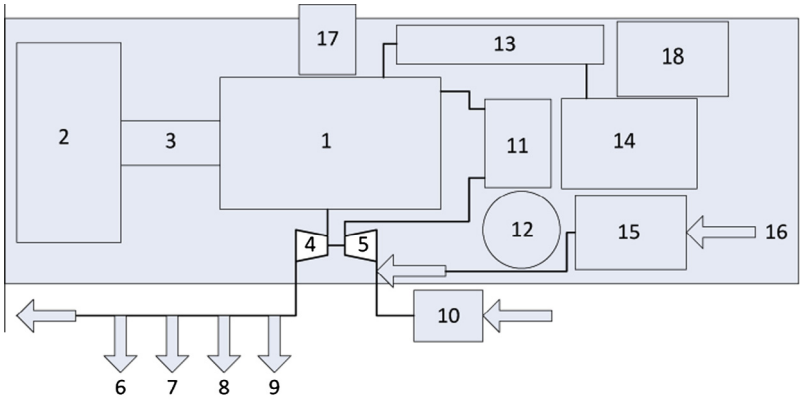

LEGEND
1: HD Engine
2: Eddy Current Dynamometer
3: Driveshaft / Cover
4, 5: Turbocharger
6: Six gas emissions bench
7: Smoke Meter
8: FTIR
9: EEPS
10: Laminar Flow Element
11: Intercooler
12: Coolant Heat Exchanger
13: Diesel Measurement
14: Diesel Storage
15: Propane Measurement
16: Propane Supply
17: Harness Adapter Board
18: Drivven / DAQ Cabinet

Fig. 1. Schematic of the experimental setup.

(DCAT). Steady state data were sampled at a rate of 2 kHz. Additional calculated channels such as mass air flow, brake power, fuel conversion efficiency, percent energy substitution (PES) of the primary fuel, overall equivalence ratio, and brake-specific emissions were recorded at a rate of 1 Hz.

3.2. High speed data acquisition

In-cylinder pressure for cylinder number 6 was measured using a Kistler 6125C piezoelectric pressure transducer that was mounted slightly recessed from the inner surface of the cylinder head in a Kistler sleeve adapter. A Kistler 5010B charge amplifier with a "short" time constant setting was used to condition the signal output from the piezoelectric pressure transducer. Diesel pressure in the high pressure fuel line between the electronic unit pump (EUP) and the injector for cylinder number 6 was measured using a Kistler 4067C3000 piezoresistive sensor and a Kistler 4618A0 amplifier was used to condition the signal. To sample the diesel pressure signal, a Kistler 6533A11 clamp-on fuel line adapter was used. Injector needle lift was unavailable; therefore, the injector command voltage was sampled for "commanded start of injection" (SOI). Transient measurements such as in-cylinder pressure, injection pressure, and injector command voltage were engine-synchronized using a BEI optical encoder with 0.1° crank angle (CAD) resolution (i.e., 3600 pulses per revolution). Cylinder pressure data were taken for 1000 consecutive engine cycles and pegged with the measured intake manifold pressure at bottom dead center (BDC). The gross apparent heat release rates (AHRR) presented in this paper were derived from measured ensemble-averaged cylinder pressure data using the following equation [33]:

$$AHRR(\theta) = \frac{\gamma}{\gamma - 1} P \frac{dV}{d\theta} + \frac{1}{\gamma - 1} V \frac{dp}{d\theta} + \frac{dQ_{ht}}{d\theta} \quad (1)$$

The instantaneous volume (V) was calculated from the known compression ratio, bore, stroke, and connecting rod length, and the pressure and volume derivatives ($dP/d\theta$ and $dV/d\theta$) were calculated numerically. The specific heat ratio (γ) was given a constant value of 1.34. Instantaneous heat transfer to the cylinder wall ($dQ_{ht}/d\theta$) was modeled using the Hohenberg correlation [34] with a constant cylinder wall temperature of 480 K.

3.3. Experimental procedure

As mentioned above, the primary objectives of the current research are to understand the impact of increased propane substitution on the performance, combustion, and exhaust emissions from the heavy-duty engine and to quantify the limits of propane substitutions over a wide range of engine loads (BMEPs from 5 to 20 bar). Consequently, for the dual fuel experiments reported in this paper unless noted otherwise, the PES of propane was slowly increased and the diesel fueling rate was correspondingly decreased while the engine load was maintained at four constant BMEP (load) conditions: 5 bar, 10 bar, 15 bar, and 20 bar. All experiments were performed at a constant engine speed of 1500 rpm, which corresponded to the highest maximum torque speed for the heavy-duty diesel engine, which had a flat peak torque curve over a range of engine speeds. Diesel injection timing, EGR valve position, and variable nozzle turbocharger (VNT) actuator position were based on the corresponding values for the "diesel-only" (0 PES) condition at each load point. The EGR valve and VNT positions varied based on the engine load but remained constant for PES sweeps at a given load. However, with increasing PES, less available energy in the exhaust gas yielded slightly lower intake boost pressures. The range of diesel injection timings were 8° to 12° before top dead center (DBTDC), the measured EGR ratios were 15–35%, and the boost pressures were 150–350 kPa. Engine coolant was supplied to the engine at 70 ± 5 °C while the coolant temperature out of the engine was maintained at 90 ± 2.5 °C. The air temperature at the outlet of the turbocharger intercooler was maintained at 31 ± 1 °C at 5 bar BMEP, 27 ± 1 °C at 10 bar BMEP, 28.5 ± 0.5 °C at 15 bar BMEP, and 30 ± 2 °C at 20 bar BMEP. The diesel fuel temperature entering the engine was controlled at 40 ± 1 °C. Since the heavy-duty diesel engine utilized a separate EUP for each cylinder, the pump timing and the pump open duration were also adjusted to the corresponding "diesel-only" values at each load. At each engine load, the diesel injection duration and the propane flow rate were adjusted to achieve the desired propane PES within ± 1 percentage points, ranging from diesel-only conditions (0 PES) to the maximum achievable PES of propane in increments of 10%. Table 2 shows the experimental matrix for the PES sweep experiments at different BMEPs. It is clearly evident that the maximum PES was dependent on BMEP. At 5 bar BMEP, the diesel injection duration could not be decreased below a certain lower limit (due to the EUP constraints), which consequently limited the maximum PES of propane to 86%. At 10, 15, and 20 bar BMEPs, high maximum pressure rise rates (MPRR) (greater than 1500 kPa/CAD) and excessive combustion noise limited the maximum PES of propane for unoptimized conditions to 60%, 33%, and 25%, respectively. However, at 10 bar BMEP alone, a limited set of experiments was performed with a different fueling strategy and with different diesel injection timings, which resulted in a maximum possible PES of 80%. It is important to note that while engine instabilities (high cyclic combustion variability) are normally encountered with conventional dual fuel combustion, especially at low loads and high PES, excessive engine instabilities were not a limiting factor in the present experiments. In fact, the measured coefficient of variation of net indicated mean effective pressure (COV of net IMEP) ranged only between 0.6% and 3.7%, with the higher values pertaining to low-load, high-PES operating conditions. On the other hand, excessive CO and HC emissions at low BMEPs further constrained the maximum PES (i.e., in addition to the injection duration limitation discussed above).

4. Definitions

Important engine parameters used in the paper such as PES, equivalence ratio (Φ), apparent ignition delay (ID_A), and EGR ratio are defined below:

$$PES = \frac{\dot{m}_g LHV_g}{\dot{m}_d LHV_d + \dot{m}_g LHV_g} \times 100\% \quad (2)$$

$$\Phi = \frac{(A/F)_{st-tot}}{\left(\frac{\dot{m}_a}{\dot{m}_d + \dot{m}_g}\right)} \quad (3)$$

$$ID_A = CA5 - SOI_{commanded} \quad (4)$$

$$EGR = \frac{CO_{2_{int}} - CO_{2_{amb}}}{CO_{2_{exh}} - CO_{2_{amb}}} \times 100\% \quad (5)$$

Table 2
Experimental test matrix for investigating PES effects at different BMEPs.

BMEP (bar)	Percent energy substitution									
	0%	10%	20%	30%	40%	50%	60%	70%	80%	86%
5	X	X	X	X	X	X	X	X	X	X
10	X	X	X	X	X	X	X	O	O	
15	X	X	X	X	33%					
20	X	X	X	25%						

Note: Data points marked by an "O" indicate additional optimization was required

In Eqs. (2) and (3), $\dot{m}$ refers to the mass flow rates of diesel (subscript d), gaseous propane fuel (subscript g), and air (subscript a), and LHV refers to the corresponding fuel lower heating values. The stoichiometric air–fuel ratio $(A/F)_{st\text{-}tot}$ is defined as the stoichiometric mass of air required for complete oxidation of a unit mass of fuel (diesel and propane) into CO_2 and H_2O. Therefore, $(A/F)_{st\text{-}tot}$ is dependent on the PES of propane. Since injector needle lift was unavailable, the $SOI_{commanded}$, which corresponds to the location at which the commanded injector voltage rises to its peak value, was used in Eq. (4) to define the SOI with the clear understanding that this may underestimate the actual SOI due to the possible "injection lag." The start of combustion is defined as CA5, or the crank angle at which 5% of cumulative heat release occurs. In Eq. (5), CO_{2int} is the CO_2 in the intake mixture, CO_{2exh} is the CO_2 in the exhaust stream, and CO_{2amb} is the CO_2 in the ambient.

An important parameter used to quantify combustion phasing is CA50, which is defined as the crank angle at which 50% of the cumulative heat release occurs. To quantify the overall combustion duration, CA10–90 is defined as the difference between the crank angle at which 10% of cumulative heat release occurs and the crank angle at which 90% of cumulative heat release occurs.

5. Results and discussion

In this section, the combustion, performance, and emissions results for diesel–ignited propane dual fuel combustion are presented. While interpreting these results, it must be noted that the maximum propane PES values are load dependent and are normally limited by high maximum pressure rise rates (MPRR) and significant audible combustion noise at high BMEPs and excessive HC and CO emissions at low BMEPs.

5.1. Combustion behavior at different BMEPs

Fig. 2(a) through (d) illustrate the crank angle-resolved AHRR for diesel–ignited propane dual fuel combustion at different engine loads (BMEPs from 5 bar to 20 bar) and at different propane percent energy substitutions (PES from 0% to 86%). Increasing propane PES has different effects on the AHRR profiles at different BMEPs. This is also reflected in the trends observed for apparent ignition delay, CA50, and CA10-90 as shown in Fig. 3 (a) through (c), respectively.

At 5 bar BMEP, two-stage AHRR profiles are observed for all PES. However, as PES is increased, the first-stage heat release decreases while the second-stage heat release increases in magnitude. This shift from first-stage to second-stage AHRR with increasing PES is accompanied by a steady increase in the apparent ignition delay (ID_A increases from 12.4 CAD at 0 PES to 15.4 CAD at 86 PES), a retardation of combustion phasing (CA50), and a decrease in combustion duration (CA10-90), as shown in Fig. 3. As the PES of propane is increased beyond 70 PES, the amount of diesel fuel is reduced very significantly compared to 0 PES, and consequently, the first-stage AHRR is decreased. In addition, an increasing percentage of propane fuel is likely burned during the second stage of combustion, thereby increasing the AHRR later in the combustion process. However, heat release ends at approximately the same crank angle for all PES, tapering off around 25° after TDC. Therefore, combined with the delayed onset of ignition, the combustion process is both retarded with respect to TDC and significantly shortened in duration (from 31.5 CAD at 0 PES to 21 CAD at 86 PES). These trends result in low fuel conversion and combustion efficiencies at high PES as discussed later.

At 10 bar BMEP, a different trend is observed. For all of the PES values investigated, the AHRR profiles illustrate single-stage heat release events. However, as PES is increased from 0 to 80%, ID_A is decreased slightly, CA50 is advanced with respect to TDC, and CA10-90 is reduced significantly. These trends are reflected in the AHRR profiles, which show a progressive advancement of the heat release and increase in the peak AHRR as PES is increased, indicating that a greater fraction of the fuel is burned early in the combustion process. At this load, cylinder pressures are higher, leading to higher in-cylinder temperatures. This increases burn rates in the propane–air mixture and results in advancing CA50 and decreasing CA10-90. For PES > 70, CA50 begins to reverse its trend and is retarded slightly; in this regard, it must be emphasized that a different fueling strategy was employed to achieve PES values higher than 60%, as discussed later. As the pilot quantity is reduced sufficiently in size, the initial heat release associated with the propane–air mixture retarded; however the peak AHRR continues to increase and CA10-90 continues to decrease.

At high loads (BMEPs of 15 and 20 bar), a third trend is observed. As PES is increased, ID_A is reduced due to higher in-cylinder temperatures and higher equivalence ratios. Moreover, CA50 is advanced with respect to TDC as PES is increased and CA10-90 is increased. At these high loads, higher bulk temperatures and high propane burn rates led to excessive MPRR, restricting the maximum PES operation at 15 bar and 20 bar BMEPs to 33% and 25%, respectively. Consequently, most of the heat release at these high loads is due to the injected diesel fuel. Despite this fact, it is clearly evident from Fig. 2(c) and (d) that increasing the PES from 0% alters the shape of the AHRR profiles from single-stage to two-stage heat release, with higher PES values leading to higher first-stage heat release. These trends indicate that the amount of propane fuel entrained in and immediately surrounding the pilot spray is increased, contributing to the higher first-stage heat release. Also, at these BMEPs, since in-cylinder temperatures are high, there is an increased tendency for propane autoignition, which can lead to engine knock.

5.2. Performance and emissions

5.2.1. Brake fuel conversion efficiency and combustion efficiency

Brake fuel conversion efficiency (FCE) trends are shown in Fig. 4(a) for various PES at all four BMEPs. For straight diesel (0 PES) operation, the FCE increases with increasing BMEP, with the only exception being 15 bar BMEP that exhibited the highest FCE among all loads studied. It must be noted that for all PES, as BMEP increases, higher exhaust enthalpy translates to higher intake boost pressures. As the PES increases at a given BMEP, the FCE behavior is affected both by the combustion phasing (CA50) and the combustion duration (CA10-90) trends. In general, as CA50 is more advanced (i.e., closer) with respect to TDC, the corresponding FCE is increased. However, if the CA50 advancement is accompanied by a decrease in CA10-90, then the resultant effects are more complex and load-dependent. For example, at 5 bar BMEP, the CA50 remains virtually invariant as PES is increased from 0% to 60% and shows a slight retardation thereafter, while CA10-90 exhibits a steady and significant decrease with PES. These trends combine to decrease the FCE as PES is increased. By comparison, at 10 bar BMEP, the CA50 is progressively advanced with PES and CA10-90 is reduced beyond 30 PES; however, the FCE slightly decreases until 30 PES and slightly increases thereafter. The FCE is nearly unaffected as PES is increased at 15 bar BMEP and shows a slight increase at 20 bar BMEP. For both 15 bar and 20 bar BMEPs, the CA50 is advanced and the CA10-90 is increased with increasing PES but the net effects on FCE are slightly different. In this regard, it is also important to remember that the maximum PES achievable at these high loads is substantially lower compared to lower loads.

Combustion efficiency is normally evaluated based on the exhaust concentrations of CO, HC, H_2 and PM emissions and their respective lower heating values [33]. Since PM concentrations in

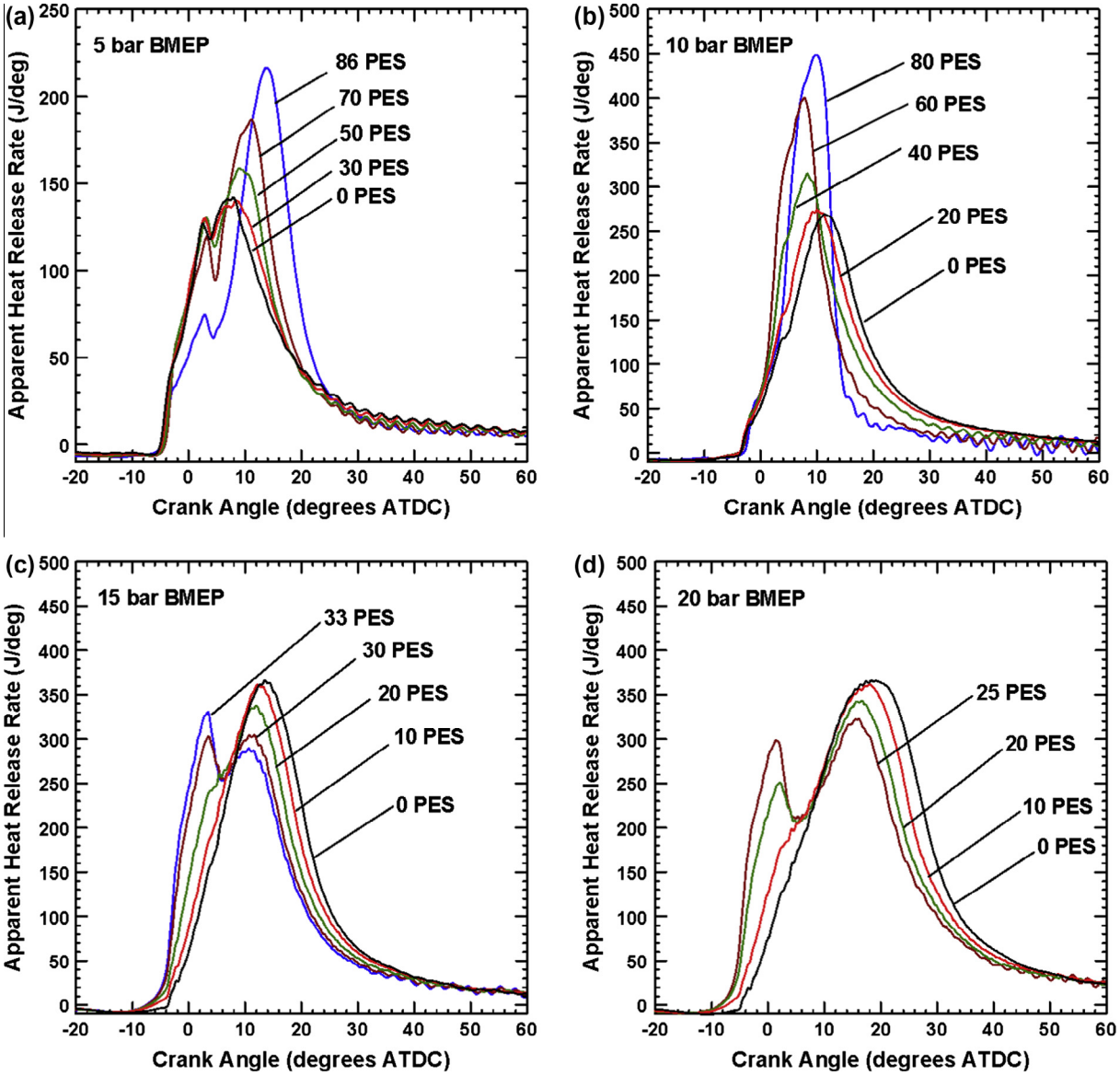

Fig. 2. Crank angle-resolved apparent heat release rates for different propane energy substitutions at (a) 5 bar BMEP, (b) 10 bar BMEP, (c) 15 bar BMEP, and (d) 20 bar BMEP.

the exhaust are not measured in the present study (instead, smoke in FSN is measured), only the measured CO and HC concentrations and the H_2 mass fractions estimated from stoichiometry are used in the combustion efficiency calculations. Following Heywood [33], the lower heating values for CO and H_2 are assumed to be 10.1 MJ/kg and 120 MJ/kg, respectively. The composition of the HC in the exhaust is not known from the FID measurements but since the lower heating values of HC are quite comparable to that of the fuel, Heywood recommends using the lower heating value of the fuel for HC in the combustion efficiency calculations. However, since two fuels are used in dual fueling, the exhaust HC can theoretically originate from both fuels; therefore, the combined mass-fraction-weighted lower heating value of "the fuel mixture" (i.e., mass-fraction-weighted average of 42.6 MJ/kg for diesel and 46.4 MJ/kg for propane) is used for the exhaust HC. The relative mass fractions of diesel and propane change with PES, and consequently, the estimated lower heating value of the exhaust HC ranges from 42.6 MJ/kg (for 0 PES) to 45.9 MJ/kg (for 86 PES). As observed in Fig. 4(b), increasing PES has a profound effect on combustion efficiency, especially at low loads. At the outset, it is evident that the combustion efficiency for straight diesel operation for all BMEPs is close to 100%. This is explained based on the fact that HC and CO emissions are very low for straight diesel operation. As PES is increased, the diesel jets become progressively smaller and more fuel is present in the lean, premixed propane–air mixture. Consequently, the highest local temperatures (~2700 K) are likely confined to increasingly smaller zones in the periphery of the diesel jets [35], where the local equivalence ratios may be close to stoichiometric ($\Phi \sim 1$) [23]. By comparison, the equivalence ratios of the premixed propane–air mixture, derived from propane and air flow measurements were consistently very lean ($0.5 < \Phi < 0.6$) for all BMEPs. At such lean premixed propane–air equivalence ratios and end-of-compression temperatures and pressures, the adiabatic combustion temperatures are estimated to be significantly lower (in the 1600–2000 K range) from adiabatic equilibrium calculations using STANJAN. It is possible that the high local temperature zones in the periphery of the diesel jets may not mix well with the cooler propane–air mixtures in the surroundings. These factors may combine to result in partial or incomplete oxidation of the fuel and CO formed during combustion, and

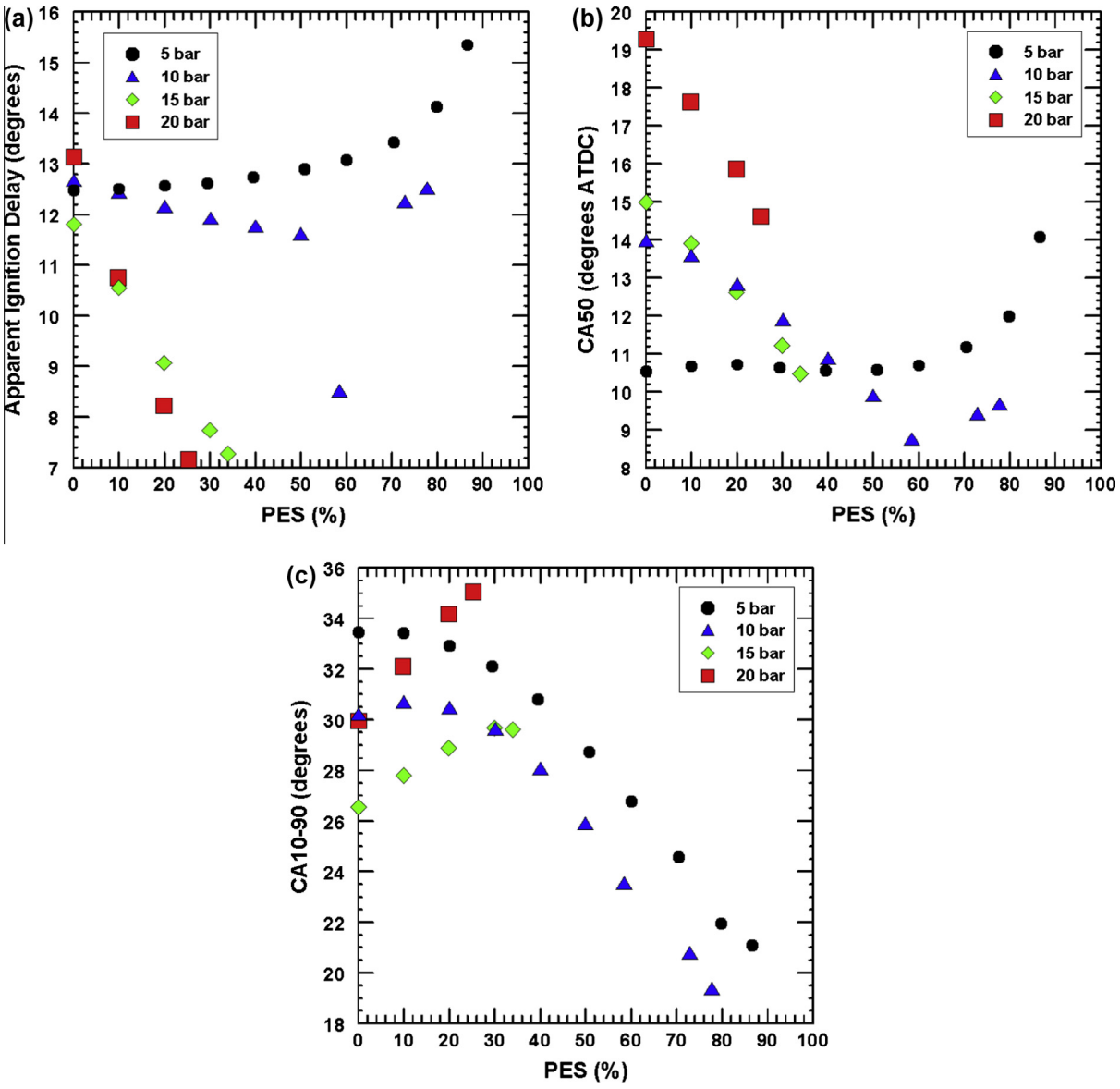

Fig. 3. (a) Apparent ignition delay, (b) CA50, and (c) CA10-90 versus propane energy substitution at various fixed BMEPs.

therefore, the HC and CO emissions are increased. Partial oxidation is more pronounced at low loads and bulk gas temperatures are lower compared to high loads, and consequently, combustion efficiency suffers more as PES is increased at 5 bar and 10 bar BMEPs.

5.2.2. NO_x and smoke emissions

Fig. 5(a) shows brake-specific NO_x emissions versus PES for 5, 10, 15, and 20 bar BMEPs. At almost all conditions, NO_x emissions decrease as PES is increased; however, the absolute magnitude of the decrease is more pronounced for higher BMEPs even though the maximum possible PES is substantially lower compared to lower BMEPs. At 5 bar BMEP, the NO_x emissions decreased from about 1.4 g/kWh at 0 PES to about 0.8 g/kWh at 86 PES. As PES is increased, the amount of diesel injected into the cylinder is decreased and the diesel jets become progressively smaller. Since the propane–air mixture surrounding the diesel jets is predominantly lean, bulk of the NO_x is likely produced in the periphery of the diesel jets where the diffusion flame is anchored, similar to conventional diesel combustion [23]. Consequently, as the PES is increased, the volume of the spatial high-temperature regions available for thermal NO production is reduced, and the overall engine-out NO_x emissions are decreased. Similar trends are observed at 15 bar and 20 bar BMEPs but the maximum NO_x reduction is limited by the maximum possible PES. At 10 bar BMEP, the NO_x emissions decrease as PES is increased up to 40% but show an increasing trend thereafter. At high PES, the increase in NO_x emissions is due to extremely rapid combustion and the associated very high peak heat release rates, which likely result in high local temperatures and increased NO_x formation.

The effect of increasing PES on smoke emissions at different BMEPs is shown in Fig. 5(b). In conventional diesel combustion, PM formation occurs in the rich premixed areas throughout the diesel jet cross-section ($2 < \Phi < 4$) and especially in the head vortex region [23]. Akihama et al. [36] showed that by reducing local temperatures below 1800 K, PM formation can be avoided even in rich premixed regions. With dual fuel combustion, especially at high PES, since the premixed propane–air mixture surrounding the diesel jet is both fuel-lean ($\Phi < 0.6$) and relatively cool (peak adiabatic equilibrium temperatures <1800 K), it does not proffer conditions conducive for PM formation. Consequently, even with dual fuel

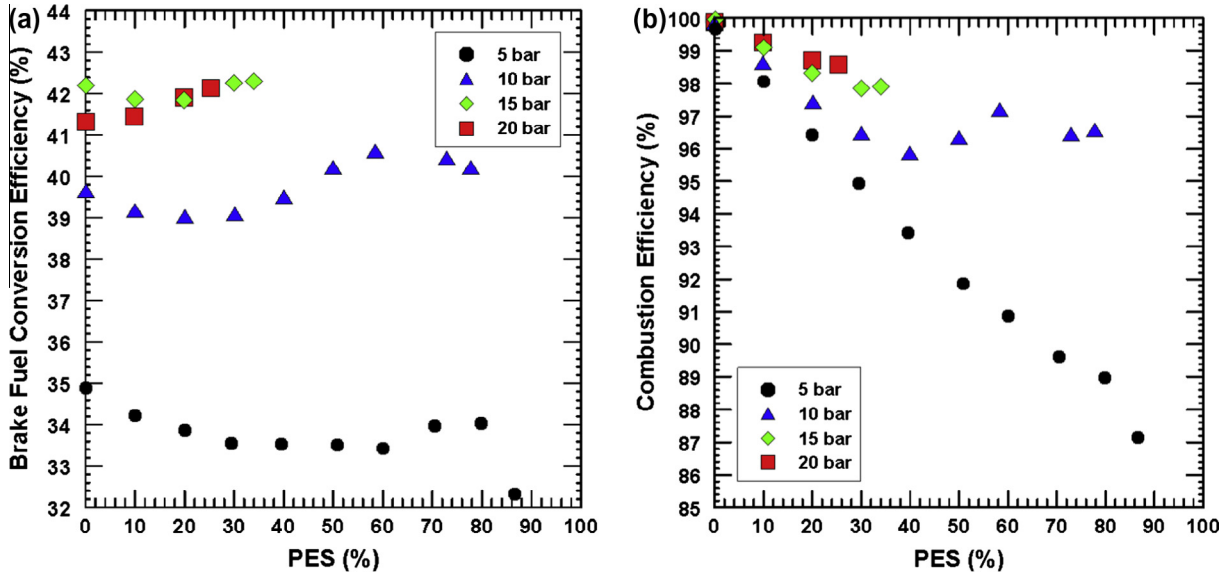

Fig. 4. (a) Brake fuel conversion efficiency (FCE) and (b) combustion efficiency versus propane energy substitution at various fixed BMEPs.

combustion, PM formation is likely restricted to the rich premixed areas throughout the diesel jet cross-section. At 5 bar BMEP, low boost pressures (~160 kPa) and high EGR ratios (~35%) are the reasons for the high smoke associated with straight diesel operation. Under these conditions, reduced in-cylinder oxygen concentrations lead to higher PM formation within the diesel jet and also inhibit PM oxidation, thereby increasing the smoke emissions for 0 PES. Increasing the PES of propane reduces the size of the diesel jet and the associated PM formation regions (locally rich premixed areas within the jet), and therefore, reduces smoke to low levels. At 10 bar BMEP, the boost pressures are higher and the EGR ratios are lower, leading to substantially lower smoke emissions (~0.7 FSN) at 0 PES. As PES is increased, the smoke emissions increase slightly until 30 PES and decrease thereafter. The following explanation is one logical, but unconfirmed, possibility. Up to 30 PES, the higher propane concentrations immediately surrounding the diesel jet may restrict oxygen availability and increase local equivalence ratios in the interior of the diesel jet, thereby increasing the *net* PM formation. Further, since the soot particles formed in the core of the diesel jet are normally oxidized in the jet periphery where there is an abundance of OH radicals in the diffusion flame, higher propane concentrations near the jet periphery may also affect PM oxidation. As PES is increased beyond 30 PES, it is possible that the decreasing size of the diesel jet and the associated PM formation regions within the jet counterbalance the aforementioned effects and reduce the net PM emissions. At 15 and 20 bar BMEPs, the boost pressures are even higher and the EGR ratios are lower, thereby decreasing the smoke emissions further at 0 PES. At 20 bar BMEP, the smoke emissions show a slightly increasing trend as PES is increased, ostensibly due to the local equivalence ratio enrichment caused by the propane entrained into the diesel jet and immediately surrounding it. By contrast, at 15 bar BMEP, the smoke emissions remain very low throughout, likely because the mutually opposing causes for PM formation (equivalence ratio enrichment versus size reduction of the PM formation regions) cancel each other.

5.2.3. CO and HC emissions

It is well-known that CO is an intermediate (stable) species formed during the oxidation process of any hydrocarbon fuel. As the oxidation process continues, CO is converted to CO_2 mostly with the aid of hydroxyl (OH) radicals that are available in high concentrations in high temperature, fuel-lean regions within the combustion chamber. This oxidation reaction ($CO + OH \rightarrow CO_2 + H$), which actually proceeds through a four-atom activated complex, is a very important exothermic reaction in hydrocarbon combustion [37]. It occurs following the oxidation of the original fuel and the intermediate hydrocarbon fragments and is relatively slow at temperatures below 1100 K [38]. Therefore, under engine combustion conditions, it is important to ensure the sustained occurrence of sufficiently high local gas temperatures (>1400 K) during and after combustion and the availability of OH radicals to facilitate CO oxidation. Fig. 5(c) shows the behavior of brake-specific CO emissions with increasing PES at different engine loads. It is clear that, for all BMEPs, the CO emissions for straight diesel operation (0 PES) are extremely low compared to the corresponding values at higher PES. In conventional diesel combustion, CO is formed within the diesel jet periphery and is oxidized almost completely within the hot diffusion flame, where there is an abundance of OH radicals and high local temperatures that accelerate CO oxidation. On the other hand, with dual fuel combustion, CO may be formed both within the diesel jet periphery as well as in the lean premixed propane–air mixture surrounding the diesel jet, which oxidizes following diesel ignition. It is likely that the CO formed within the diesel jet is largely oxidized in the jet periphery while only a portion of the CO formed in the propane–air mixture is oxidized within the cylinder. As PES is increased up to a certain BMEP-dependent value, substantial fractions of the CO formed in the lean, premixed propane-air mixture may remain unoxidized until the exhaust valve opens for the following possible reasons: (1) reduced availability of OH radicals required for CO oxidation due to relatively low local combustion temperatures in the propane–air mixture, (2) inadequate mixing between the high temperature zones within the diesel jets (which become progressively smaller with increasing PES) and the low temperature zones in the propane–air mixture, and (3) reduced time available for CO oxidation due to shorter combustion durations, i.e., CO oxidation freezes quickly after combustion ends.

At 5 bar BMEP, the CO emissions increase up to 60 PES and decrease for higher PES values. The initial increase in CO emissions is associated with the increase in CO formation in the lean propane–air mixture. Another factor that may contribute to the

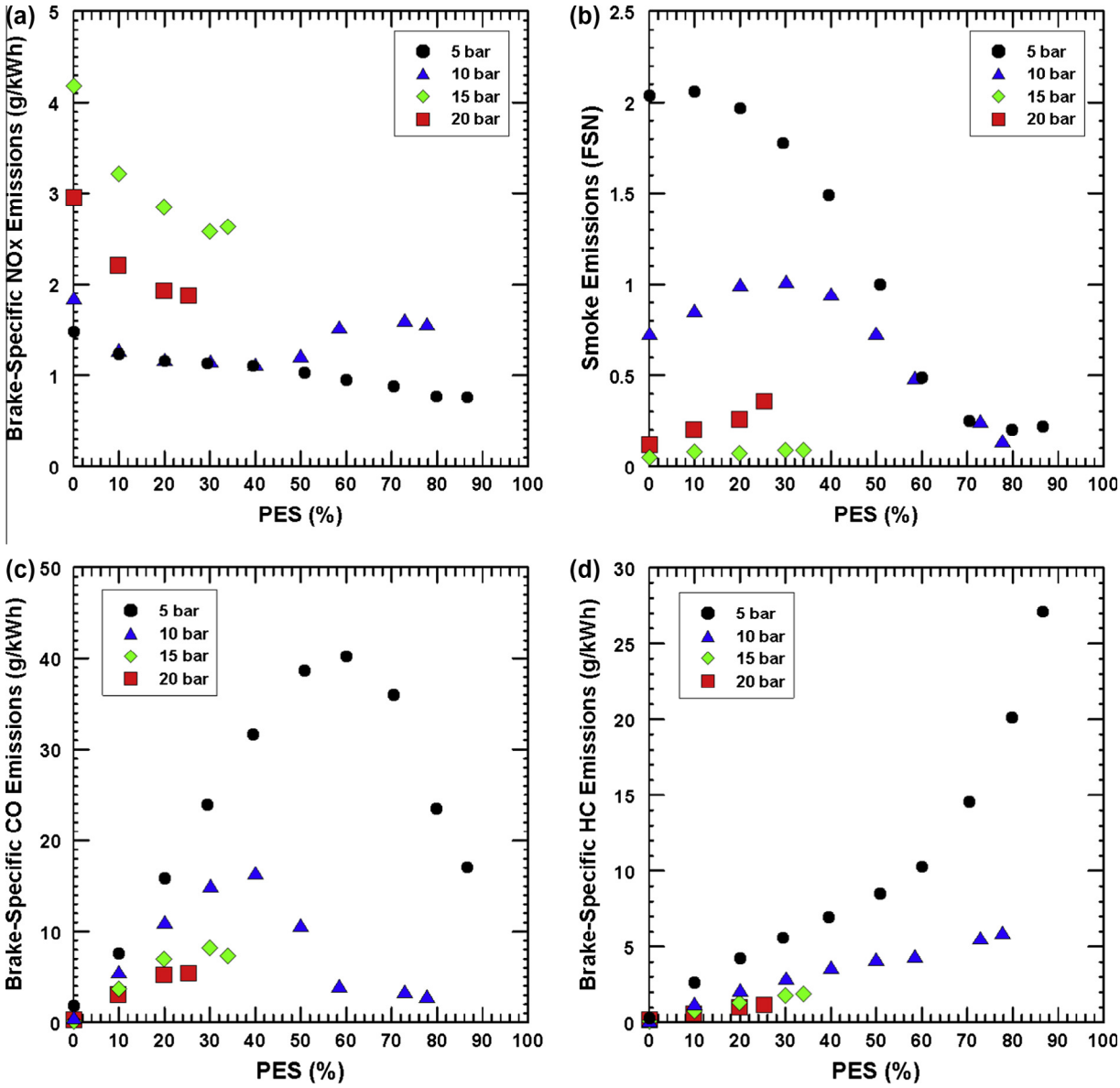

Fig. 5. (a) Brake-specific NO_x emissions, (b) smoke emissions, (c) brake-specific CO emissions, and (d) brake-specific HC emissions versus propane energy substitution at various fixed BMEPs.

high CO values with dual fuel combustion is the reduction in combustion duration (CA10-90) with increasing PES at low loads. Decreasing CA10-90 implies that the combustion process is over relatively quickly, the post-combustion gases cool down faster, and consequently, the time available for CO oxidation is reduced, thereby increasing engine-out CO emissions in general. The CO reduction beyond 60 PES can be explained as follows. Since CO oxidation occurs much later in the combustion process (following oxidation of the original fuel and the intermediate hydrocarbon fragments), the HC and CO emissions are interdependent, especially for dual fuel combustion. At 5 bar BMEP, as PES is increased beyond 60 PES, the HC emissions continue to increase (see Fig. 5(d)), while CO emissions decrease. These trends are related to each other because at high PES, the original fuel and the intermediate hydrocarbon fragments (which constitute the unburned HC emissions) are not oxidized likely due to relatively low temperatures in the lean propane–air mixture and ineffective mixing of the hotter regions in the diesel jet with the surroundings. Therefore, the in-cylinder CO formation itself is reduced and the engine-out CO emissions decrease. Another possible contributor to the CO reduction at high PES is the relatively higher peak bulk gas temperatures, evaluated from the measured cylinder pressure histories by applying the ideal gas equation of state, (~1250 K at 86 PES compared to ~1150 K at 0 PES) that may enhance the CO oxidation process. Finally, under conditions that favor premixed flame propagation in dual fuel combustion, flame quenching may also affect CO emissions through the complex interplay between HC (fuel) oxidation rates and CO formation and oxidation rates.

At 10 bar BMEP, a similar but significantly lower CO peak is observed at 40 PES. For PES values higher or lower than 40 PES, the CO emissions are lower for the same reasons as discussed above for 5 bar BMEP. In general, at 10 bar BMEP, the in-cylinder bulk gas temperatures and the local equivalence ratios are relatively higher, thereby reducing the overall CO emissions compared to 5 bar BMEP. The CO emissions show a slightly increasing trend at higher BMEPs (15 and 20 bar) but the overall magnitudes are

lower compared to 5 and 10 bar BMEPs. Again, this may be attributed to substantially higher in-cylinder bulk gas temperatures and higher OH radical concentrations, which facilitate CO oxidation at higher BMEPs. In addition, since the maximum PES was restricted only to 33% and 25%, respectively at 15 and 20 bar BMEPs, the CO peaks evident at lower loads are not readily observed.

Fig. 5(d) shows the behavior of brake-specific HC emissions at different PES for different BMEPs. Similar to CO emissions, the HC emissions are very low for straight diesel operation (0 PES) at all loads. Clearly, either very little unburned fuel escapes the diffusion flame or most of the intermediate hydrocarbon fragments are oxidized in the relatively hot post-combustion gases in conventional diesel combustion, as evident from the low engine-out HC emissions. By comparison, for dual fuel combustion, the HC emissions increase steadily as PES is increased at all BMEPs. Karim [39] attributes the high HC emissions in dual fuel combustion to incomplete flame propagation, i.e., the flame initiated by the ignited pilot spray cannot spread sufficiently far or sufficiently fast to burn all of the gaseous fuel–air mixture despite the presence of excess oxygen. Moreover, high HC emissions may also be attributed to the propane–air mixture trapped in crevices around the combustion chamber that may be left unburned at the end of the combustion process. It is also possible that HC oxidation is hampered by relatively low temperatures in the lean propane–air mixture present in the combustion chamber (outside the crevices) and inadequate mixing of the hotter regions in the diesel jet with the surroundings. From Fig. 5(d), it is clear that HC emissions (like CO emissions) are more significant at low loads and high PES. These trends might be explained based on the following observations. First, as PES is increased at low loads, the amount of propane trapped in crevices and present in the lean propane–air mixture increases. At high PES, the propane trapped in these regions is either partially converted to intermediate hydrocarbon fragments or remains completely unburned until the exhaust valve opens, thus resulting in high engine-out HC emissions. Second, at low loads, the bulk gas temperatures that facilitate HC oxidation are relatively lower compared to high loads. For example, the peak bulk gas temperatures are 1250 K at 5 bar BMEP and 86 PES, 1450 K at 10 bar BMEP and 80 PES, 1430 K at 15 bar BMEP and 33 PES, and 1460 K at 20 bar BMEP and 25 PES. Third, mixing of the high temperature diesel combustion zones with the leaner, low temperature propane combustion zones may be inhibited at high PES for all BMEPs. This may explain why the HC emissions are higher at high PES for a given BMEP despite the fact that the peak bulk gas temperatures are uniformly higher at high PES (e.g., for 10 bar BMEP, the peak bulk gas temperatures are 1240 K at 0 PES and 1450 K at 80 PES). Consequently, the HC oxidation process is severely inhibited at low loads and high PES, thereby increasing the engine-out HC emissions.

5.2.4. Particle number concentrations and size distributions

Figs. 6(a) through (d) illustrate the exhaust particle number concentrations (normalized with particle diameter to yield $dN/d\log D_p$ in number of particles per cubic centimeter) versus particle diameter (D_p) for different propane PES and BMEPs from 5 bar to 20 bar. Both the shapes of the particle number concentration curves as well as the trends with increasing propane PES are clearly load-dependent. For instance, as the BMEP is increased from 5 bar to 20 bar, the particle number concentration curves change from being unimodal to bimodal. At 5 bar BMEP, as propane substitution is increased from 0 PES to 86 PES, the particle concentrations decrease by more than one order of magnitude (please note the log scale on the ordinate). This trend is consistent with the smoke trends shown in Fig. 5(b) for 5 bar BMEP. As mentioned before, one of the concerns with dual fueling is to understand if the reduction in smoke emissions at high PES is accompanied by a commensurate increase in particle number concentrations in the ultrafine or nanoparticle regime. At 5 bar BMEP, both the smoke and particle number concentrations are reduced at high PES. At 10 bar BMEP, the peak particle number concentrations are much lower (even for 0 PES) compared to 5 bar BMEP. However, the overall trends are similar to 5 bar BMEP in the fact that the particle number concentrations are reduced as PES is increased from 0 to 80 PES. By contrast, for 15 and 20 bar BMEPs, the opposite trends are observed. As PES is increased at these high loads, the particle number concentrations are are increased from the straight diesel (0 PES) values. These trends are also consistent with the increased smoke emissions observed at high loads as PES is increased. In addition, the overall magnitudes of the particle concentrations are lower compared to the low load conditions. This may be explained based on the fact that higher boost pressures and lower EGR ratios are used at high BMEPs for all PES. It is also important to note that the maximum possible PES values at 15 and 20 bar BMEPs are only 33 and 25 PES, respectively. Therefore, from these results, it is not quite clear if the particle concentrations will continue to increase at higher PES (if they were somehow possible) or if the trends would be reversed.

5.2.5. Maximum pressure rise rate and combustion noise

An important concern in dual fuel combustion is the potential for high maximum pressure rise rates (MPRR) and combustion noise, eventually manifesting as engine knock when PES is increased, especially at high loads. Fig. 7(a) and (b) show the MPRR and combustion noise (derived from cylinder pressure measurements using the DCAT software) trends at different BMEPs and different PES. For straight diesel operation (0 PES) at all BMEPs, the MPRR lies in the range of 500–600 kPa/CAD. On the other hand, as BMEP is increased from 5 bar to 20 bar at 0 PES, the combustion noise is reduced from about 86 decibels (dB) to about 79 dB, likely due to the reduction in the first-stage heat release as BMEP is increased.

As PES is increased at 5 bar BMEP, the MPRR variations are negligible until about 40 PES. Between 40 and 70 PES, the MPRR increases slightly but decreases at higher PES. Correspondingly, the combustion noise varies between 86 and 90 dB over the entire range of PES investigated at 5 bar BMEP. As evident from Fig. 2(a), when PES is increased up to 30 PES, the AHRR curves are not affected significantly, which explains the negligible MPRR and combustion noise variations. However, at higher PES, the first stage of heat release is diminished as the diesel quantity is reduced while the magnitude of the second stage of AHRR is increased. These effects combine to result in the slight increase in MPRR and combustion noise at high PES. For the highest PES value of 86 PES, the MPRR and combustion noise are reduced because the CA50 is delayed significantly compared to 0 PES. At 10 bar BMEP, a steady increase in MPRR is observed as PES is increased from 0 to 40 PES, while beyond 40 PES, the MPRR increase is very sharp and reaches a maximum of 2500 kPa/CAD at 80 PES. It must be noted that the last two data points (the two highest PES values) at 10 bar BMEP were obtained during the propane PES improvement tests described below. The combustion noise increases from about 85 dB at 0 PES to a maximum of 100 dB at 80 PES at this load. This sharp increase in MPRR and combustion noise at 10 bar BMEP is also associated with the steep increase in the first-stage heat release as evident from Fig. 2(b). By comparison, for the higher BMEPs of 15 and 20 bar, the increase in MPRR and combustion noise with increasing PES is even more pronounced compared to 5 and 10 bar BMEPs despite the fact that the maximum PES is limited to only 33% and 25%, respectively. These trends can be understood from the fact that for both 15 and 20 bar BMEPs the first-stage heat release, which is virtually absent at 0 PES, increases as PES is increased. Higher first-stage heat release at these high loads leads to higher MPRR and rougher engine operation even at fairly low propane substitutions.

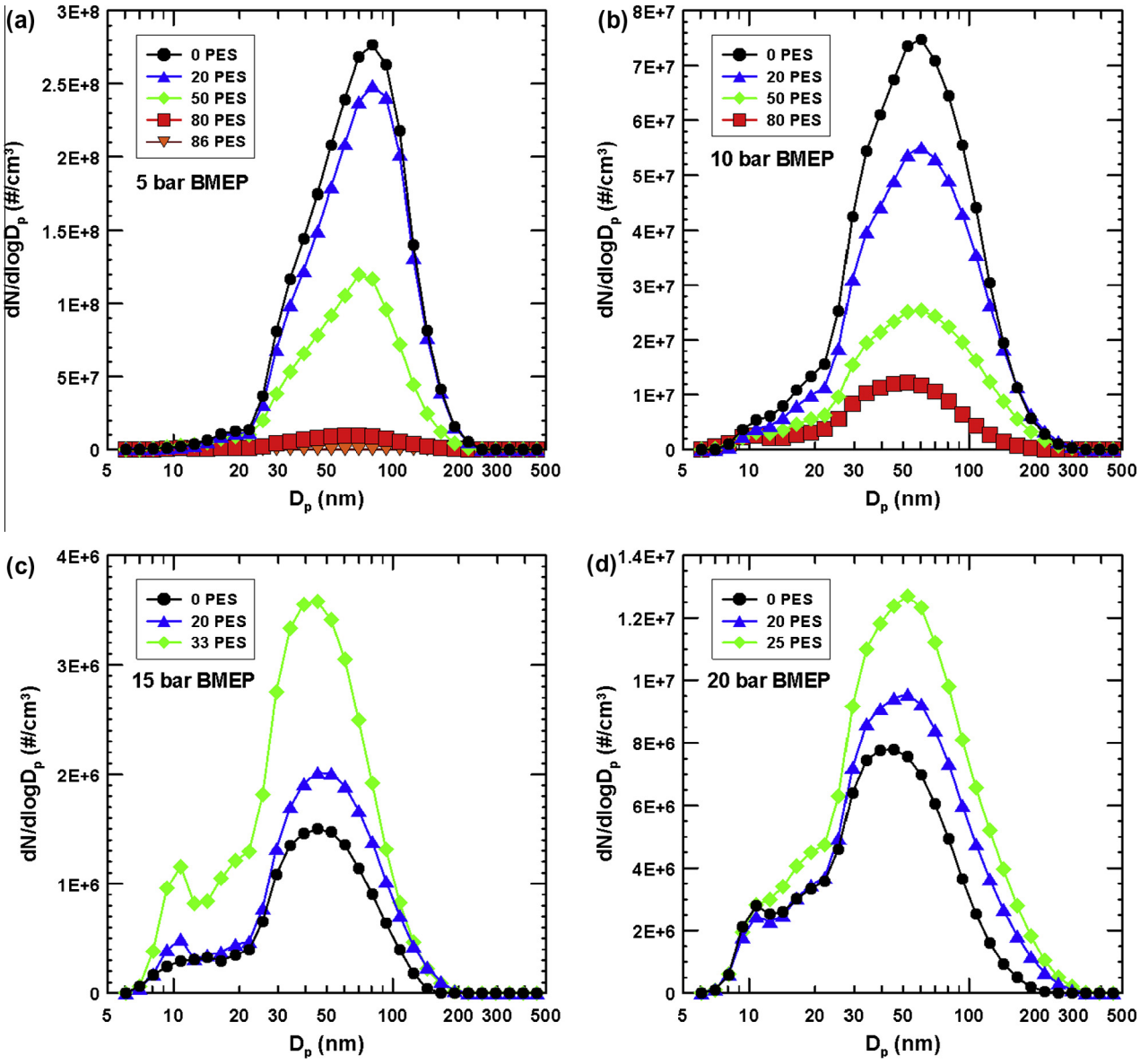

Fig. 6. Normalized particle number concentrations ($dN/d\log D_p$) measured at the engine exhaust for different propane energy substitutions at (a) 5 bar BMEP, (b) 10 bar BMEP, (c) 15 bar BMEP, and (d) 20 bar BMEP.

5.3. Experiments to improve propane PES at 10 bar BMEP

5.3.1. Fueling strategy

In the MPRR plot shown in Fig. 7(a), stock engine parameters are used for 10 bar BMEP up to 60 PES. Higher PES values of propane are achieved with a different fueling strategy as discussed below. At 10 bar BMEP, the MPRR increased until it reached fairly high values (above 1500 kPa/CAD) as PES is increased to 60%. This steep increase in MPRR is related to the second-stage heat release and the relatively higher contribution to AHRR from propane compared to diesel at higher PES. At 30 PES of propane, a shift in the crank angle-resolved location of MPRR occurs (not shown); i.e., at low PES, the MPRR occurs during the first-stage heat release while above 30 PES the MPRR occurs during the second-stage heat release. Compared to 5 bar BMEP, the higher in-cylinder pressures at 10 bar BMEP yield higher bulk temperatures and cause the propane–air mixture to burn more quickly, resulting in higher heat release rates. At 15 and 20 bar BMEPs, the shift in MPRR location from the first to second stage of heat release occurs progressively earlier in terms of increasing propane PES (i.e., for a more modest increase in PES).

To suppress the high heat release rates at 10 bar BMEP and to increase propane substitution beyond 60 PES, a different fueling strategy was required. Instead of gradually decreasing the diesel pilot and increasing propane concentration while keeping the engine load at 10 bar BMEP, the operating conditions are achieved by first operating the engine with a desired pilot quantity calculated for a desired propane PES, and subsequently, increasing the propane substitution to reach the desired load of 10 bar BMEP. This strategy is chosen to reduce the pilot quantity, thereby reducing in-cylinder temperatures during transient operation while achieving the desired steady state operating point. By adopting this fueling strategy, the maximum PES of propane at 10 bar BMEP is increased to 80%, as denoted by the "O" data points in Table 2. A lower pilot quantity permitted a higher PES to be achieved by delaying the rapid rise in MPRR. The maximum propane substitution was again limited to 80 PES by high MPRR and excessive combustion noise due to rapid heat release as

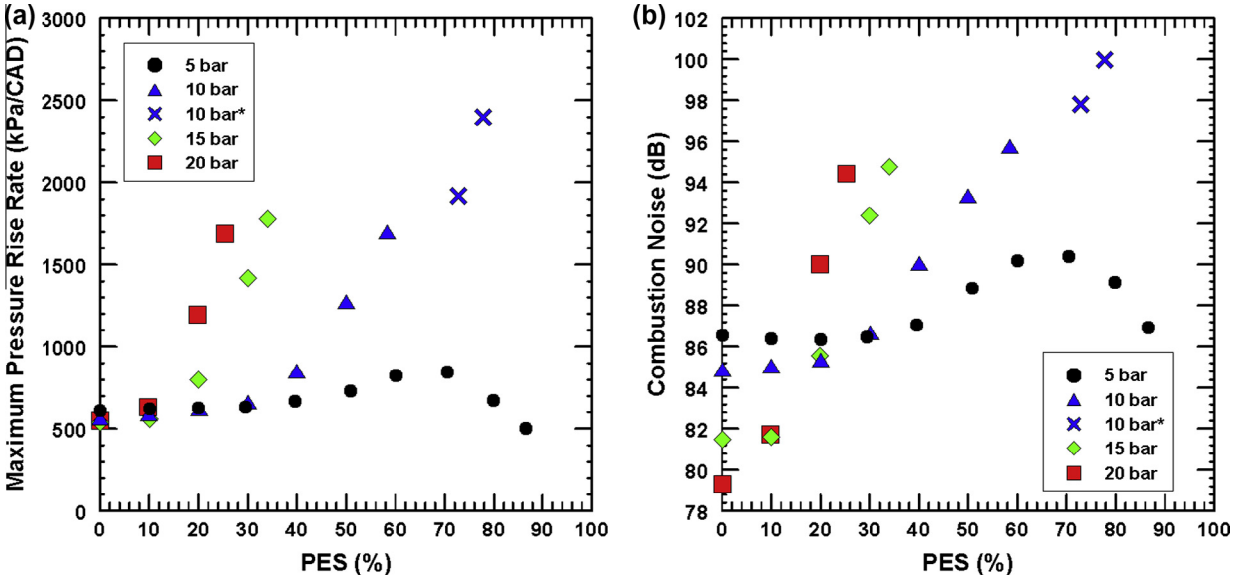

Fig. 7. (a) Maximum pressure rise rate (MPRR) and (b) combustion noise (derived from measured cylinder pressures) versus propane energy substitution at various fixed BMEPs.

evident from Fig. 7. Engine operation at 70 and 80 PES might be viewed as quasi-steady or metastable because slight changes in operating parameters led to engine runaway, unacceptably high MPRR values, and very rough engine operation.

5.3.2. Diesel injection timing study

To reduce the MPRR at 10 bar BMEP and 80 PES of propane, the influence of diesel injection timing is investigated over a limited range near TDC. For these experiments, the Drivven engine controller is used to provide control over the commanded SOI. Injection timings range from the timing of 8.6 DBTDC to 2.6 DBTDC in 1° increments. As the injection timing is retarded, the peak pressure is reduced until 6.6 DBTDC, as shown in Fig. 8(a). Moreover, as evident from Fig. 8(b), MPRR is decreased as injection timing is retarded up to 6.6 DBTDC because the MPRR location (MPRR-L) shifts back to the first stage of heat release. This is due to the second stage of heat release occurring later in the expansion stroke, resulting in lower peak pressures, lower bulk temperatures, and lower fuel conversion efficiencies. Retarding the injection timing beyond 6.6 DBTDC leads to an increase in peak heat release rate as well as a slight advancement of the peak heat release location with respect to TDC. This trend may appear counterintuitive but may be explained as follows. Retarding the injection timing beyond 6.6 DBTDC results in progressively higher exhaust enthalpy available at the inlet to the turbocharger turbine. For a fixed turbocharger VNT position, this translates to higher boost pressures, and therefore, higher temperatures in the unburned propane–air mixture surrounding the diesel jets. Higher unburned mixture temperatures result in faster second-stage heat release rates, which are mostly associated with propane combustion. When injection timing is sufficiently delayed (2.6 DBTDC), high intake boost pressures result in a second stage of heat release that is similar to that obtained for 8.6 DBTDC timing. In turn, this results in a significant increase in MPRR as shown in Fig. 8(b) because the MPRR-L is shifted back to the second stage of heat release. The high MPRR value (~1400 kPa/CAD) experienced at 2.6 DBTDC timing prevented engine operation at more retarded injection timings. Efficiency and emissions results obtained in these injection timing studies for 10 bar BMEP are shown in Table 3. As the commanded SOI is retarded from 8.6 (baseline) to 2.6 DBTDC, the FCE decreases

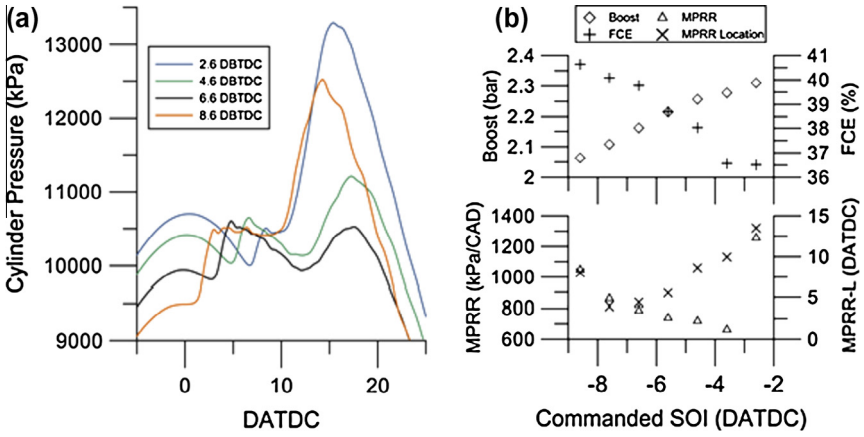

Fig. 8. (a) Cylinder pressure histories for different commanded SOIs and (b) FCE, MPRR, location of MPRR (MPRR-L), and intake boost pressure versus commanded SOI for BMEP = 10 bar, PES = 80%, T_{in} = 26.8 °C.

Table 3
Efficiency, combustion, and emissions results from diesel injection timing experiments at 10 bar BMEP.

Commanded SOI (DBTDC)	FCE (%)	Combustion efficiency (%)	CA50 (DATDC)	NO_x (g/kWh)	HC (g/kWh)	CO (g/kWh)
8.6	40.2	96.6	12.9	1.56	5.96	2.93
7.6	40.1	96.3	14.9	1.24	7.62	4.96
6.6	39.8	96.0	16.3	1.07	8.40	7.10
5.6	38.7	95.5	16.7	0.91	9.71	10.61
4.6	38.0	95.2	16.4	0.84	10.48	13.10
3.6	36.6	94.6	17.2	0.74	12.67	17.37
2.6	36.5	94.7	14.3	0.80	12.34	17.41

from 40.2% to 36.5% while the combustion efficiency decreases from 96.6% to 94.7%, respectively. Correspondingly, when the commanded SOI is retarded, the NO_x emissions decrease from 1.56 g/kWh to 0.80 g/kWh while the HC emissions increase from 5.96 g/kWh to 12.34 g/kWh and CO emissions increase from 2.93 g/kWh to 17.41 g/kWh. The decrease in NO_x emissions can be explained based on the delayed CA50 and likely lower local temperatures within the diesel jets during and after the end of combustion for retarded injection timings. The measured smoke emissions remain virtually invariant (~0.1 FSN) with injection timing within this range probably due to the high propane PES (80 PES) at all SOIs and the associated lower pilot quantities and fewer locally fuel-rich areas during combustion. On the other hand, when the commanded SOI is retarded from 8.6 to 2.6 DBTDC, the HC and CO emissions increase likely due to a combination of reduced time available for HC and CO oxidation (both during and after combustion) and relatively poor mixing between the high-temperature diesel combustion zones and low-temperature propane–air combustion zones for late SOIs and delayed CA50. Based on the tradeoffs observed between the measured MPRR, FCE, and emissions, the commanded SOI of 6.6 DBTDC appears to be the optimal choice within this range of SOIs with MPRR ~ 790 kPa/CAD, FCE ~ 39.8%, 96% combustion efficiency, NO_x ~ 1 g/kWh, HC ~ 8.4 g/kWh, and CO ~ 7.1 g/kWh.

6. Conclusions

Diesel–ignited propane dual fuel combustion was characterized experimentally on a 12.9-l, heavy duty diesel engine. The first set of experiments utilized stock control parameters to quantify the effects of varying percent energy substitution (PES) of propane at four different brake mean effective pressure (BMEP) conditions of 5, 10, 15, and 20 bar at a fixed maximum torque speed of 1500 rpm. At 10 bar BMEP alone, a second set of experiments was performed with a Drivven open-architecture engine controller to improve propane PES and to limit the maximum pressure rise rate (MPRR) by altering the fueling strategy and the commanded diesel injection timing (SOI). Analysis of the results obtained in these experiments leads to the following important conclusions:

1. For unoptimized conditions with stock engine control parameters, the maximum possible propane PES values were limited to 86% at 5 bar BMEP due to excessive HC and CO emissions and diesel injection duration limitations, and to 60%, 33%, and 25% at 10, 15, and 20 bar BMEPs, respectively, due to high MPRRs (>1500 kPa/CAD) and excessive combustion noise (95–100 dB).
2. Two-stage apparent heat release rate (AHRR) profiles were observed for all PES at 5 bar BMEP while higher loads exhibited single stage AHRR, which was altered to two-stage AHRR as PES was increased. Increasing PES typically increased the second-stage AHRR at low loads but increased both first- and second-stage AHRR at higher loads. With increasing PES at low loads, the apparent ignition delay (ID_A) steadily increased, CA50 was retarded, and CA10-90 was decreased. At higher loads, the ID_A generally decreased and CA50 was advanced with increasing PES, while CA10-90 was more dependent on the maximum possible PES at a given load.
3. As PES was increased at a given BMEP, the brake fuel conversion efficiency (FCE) was typically increased if CA50 was closer to TDC; however, if the CA50 advancement was accompanied by a decrease in CA10-90, the FCE trends became more complex and load-dependent. By comparison, while combustion efficiencies exhibited only slight reductions (from near 100% at 0 PES to about 96% at higher PES) at high loads, they suffered significantly at 5 bar BMEP decreasing from near 100% at 0 PES to 87% at 86 PES.
4. At all BMEPs, engine-out NO_x emissions decreased as PES was increased; however, the absolute magnitude of the decrease was more pronounced for higher BMEPs. On the other hand, while smoke emissions decreased with increasing PES for 5 and 10 bar BMEPs, they remained invariant or showed a slight increase with PES at 15 and 20 bar BMEPs.
5. Brake-specific HC emissions increased with increasing PES at all loads but these trends were especially significant at 5 bar BMEP (from 0.3 g/kWh at 0 PES to 27 g/kWh at 86 PES). The CO emissions also increased with increasing PES at all loads but for 5 bar and 10 bar BMEPs, the CO emissions decreased as PES was increased beyond certain critical PES values (60 PES for 5 bar and 40 PES for 10 bar BMEP).
6. Exhaust particle number concentration ($dN/d\log D_p$) measurements yielded trends dependent on both load and PES. As BMEP was increased from 5 bar to 20 bar, the $dN/d\log D_p$ curves changed from being unimodal to bimodal. While $dN/d\log D_p$ decreased significantly with increasing PES at 5 bar and 10 bar BMEPs, the trends were reversed at higher loads, consistent with the increasing smoke trends with increasing PES at the higher loads.
7. At 10 bar BMEP, by starting with a low, pre-calculated pilot quantity and by increasing the propane flow rate to reach the desired load, the maximum possible propane PES was extended to 80%, albeit for quasi-steady engine operation. The SOI studies (from 2.6 to 8.6 DBTDC) yielded the optimal efficiency-emissions-MPRR tradeoff for the SOI of 6.6 DBTDC at 10 bar BMEP.

7. Disclaimer

The material and other information included in this publication are intended to provide general guidance only on the subject matter addressed by the publication. It is not intended to be a substitute for the personal instruction, guidance, and advice of a professional with training and experience in the safe and proper use of propane.

Acknowledgments

This paper is based upon research funded by the Propane Education and Research Council (PERC, Docket No. 16555) and performed at Mississippi State University. The authors gratefully acknowledge facilities support from the Center for Advanced Vehicular Systems at Mississippi State University. The views and opinions expressed herein are not necessarily those of the sponsoring agency or of the university.

References

[1] US EPA Heavy-Duty Engine Emissions standards. <http://www.dieselnet.com/standards/us/hd.php> [accessed 08.12.13].
[2] Karim GA. The dual fuel engine. In: Evans RL, editor. Automotive engine alternatives. Plenum Press; 1987.

[3] Stewart J, Clarke A, Chen R. An experimental study of the dual-fuel performance of a small compression ignition diesel engine operating with three gaseous fuels. Proc Inst Mech Engrs Part D: J Automob Eng 2007;221(8):943–56.
[4] Weaver CS, Turner HS. Dual fuel natural gas/diesel engines: technology, performance, and emissions. SAE paper 940548; 1994.
[5] Karim GA. Combustion in gas fueled compression–ignition engines of the dual fuel type. Trans ASME: J Eng Gas Turb Power 2003;125:827–36.
[6] Shoemaker NT, Gibson CM, Polk AC, Krishnan SR, Srinivasan KK. Performance and emissions characteristics of bio-diesel (B100)-ignited methane and propane combustion in a four cylinder turbocharged compression ignition engine. ASME: Trans J Eng Gas Turb Power 2012;134(8):082803. http://dx.doi.org/10.1115/1.4005993. 10p.
[7] Ryu K. Effects of pilot injection pressure on the combustion and emissions characteristics in a diesel engine using biodiesel–CNG dual fuel. Energy Convers Manage 2013;76:506–16.
[8] Lu X, Ma J, Ji L, Huang Z. Simultaneous reduction of NO_x emission and smoke opacity of biodiesel-fueled engines by port injection of ethanol. Fuel 2008;87:1289–96.
[9] Chen Z, Yao M, Zheng Z, Zhang Q. Experimental and numerical study of methanol/dimethyl ether dual-fuel compound combustion. Energy Fuels 2009;23:2719–30.
[10] Korakianitis T, Namasivayam AM, Crookes RJ. Natural-gas fueled spark-ignition (SI) and compression–ignition (CI) engine performance and emissions. Prog Energy Combust Sci 2011;37(1):89–112. http://dx.doi.org/10.1016/j.pecs.2010.04.002.
[11] Krishnan SR, Biruduganti M, Mo Y, Bell SR, Midkiff KC. Performance and heat release analysis of a pilot-ignited natural gas engine. Int J Engine Res 2002;3(3):171–84.
[12] Ishiyama T, Shioji M, Mitani S, Shibata H. Improvement of performance and exhaust emissions in a converted dual-fuel natural gas engine. SAE paper 2000-01-1866; 2000.
[13] Papagiannakis RG, Hountalas DT. Combustion and exhaust emission characteristics of a dual fuel compression ignition engine operated with pilot diesel fuel and natural gas. Energy Convers Manage 2004;45:2971–87.
[14] Papagiannakis RG, Rakopoulos CD, Hountalas DT, Rakopoulous DC. Emission characteristics of high speed, dual fuel, compression ignition engine operating in a wide range of natural gas/diesel fuel proportions. Fuel 2010;89(7):1397–406.
[15] Carlucci AP, Laforgia D, Saracino R, Toto G. Combustion and emissions control in diesel–methane dual fuel engines: the effects of methane supply method combined with variable in-cylinder charge bulk motion. Energy Convers Manage 2011;52(8–9):3004–17.
[16] Mustafi NN, Raine RR, Verhelst S. Combustion and emissions characteristics of a dual fuel engine operated on alternative gaseous fuels. Fuel 2013;109:669–78.
[17] Korakianitis T, Namasivayam AM, Crookes RJ. Diesel and rapeseed methyl ester (RME) pilot fuels for hydrogen and natural gas dual–fuel combustion in compression–ignition engines. Fuel 2011;90:2384–95.
[18] Polk AC, Gibson CM, Shoemaker NT, Srinivasan KK, Krishnan SR. Detailed characterization of diesel–ignited propane and methane dual fuel combustion in a turbocharged DI diesel engine. Proc IMechE Part D: J Automob Eng 2013;227(9):1255–72. http://dx.doi.org/10.1177/0954407013487292.
[19] Goldsworthy L. Combustion behavior of a heavy duty common rail marine diesel engine fumigated with propane. Exp Thermal Fluid Sci 2012;42:93–106.
[20] Kajiwara M, Sugiyama K, Sagara M, Mori M, Goto S, Alam M. Performance and emissions characteristics of an LPG direct injection diesel engine. SAE paper 2002–01-0869, 2002.
[21] Jian D, Xiaohong G, Gesheng L, Xintang Z. Study on diesel–LPG dual fuel engines. SAE paper 2001-01-3679; 2001.
[22] Poonia MP, Ramesh A, Gaur RR. Experimental investigation of the factors affecting the performance of a LPG – diesel dual fuel engine. SAE paper 1999-01-1123; 1999.
[23] Dec JE. A conceptual model of DI diesel combustion based on laser-sheet imaging. SAE paper 970873; 1997.
[24] Prikhodko VY, Curran SJ, Barone TL, Lewis SA, Storey JM, Cho K et al. Diesel oxidation catalyst control of hydrocarbon aerosols from reactivity controlled compression ignition combustion. Paper IMECE2011-64147, ASME 2011 international mechanical engineering congress and exposition, Denver, Colorado, USA, 11–17 November 2011.
[25] Prikhodko VY, Curran SJ, Barone TL, Lewis SA, Storey JM, Cho K, et al. Emission characteristics of a diesel engine operating with in-cylinder gasoline and diesel fuel blending. SAE Int J Fuels Lubr 2010;3(2):946–55. also SAE paper 2010-01-2266.
[26] Zhou L, Liu Y-F, Wu C-B, Sun L, Wang L, Zeng K, et al. Effect of the diesel injection timing and the pilot quantity on the combustion characteristics and the fine-particle emissions in a micro-diesel pilot-ignited natural-gas engine. Proc IMechE, Part D: J Automob Eng 2013;227(8):1142–52. http://dx.doi.org/10.1177/0954407013480452.
[27] Liu Z, Karim GA. Knock characteristics of a dual fuel engine with hydrogen fuel. Int J Hydrogen Energy 1995;20(11):919–24.
[28] Srinivasan KK, Krishnan SR, Midkiff KC. Improving low load combustion, stability and emissions in pilot-ignited natural gas engines. Proc Instn Mech Engrs: Part D, J Automob Eng 2006;220(2):229–39.
[29] Liu Z, Karim GA. An examination of the ignition delay period in gas-fueled diesel engines. Trans ASME: J Eng Gas Turb Power 1998;120:225–31.
[30] Polk AC, Gibson CM, Shoemaker NT, Srinivasan KK, Krishnan SR. Analysis of ignition behavior in a dual fuel turbocharged direct injection engine using propane and methane as primary fuels. Trans ASME: J Energy Resour Technol 2013;135(3):032202. http://dx.doi.org/10.1115/1.4023482. 10p.
[31] Gibson CM, Polk AC, Shoemaker NT, Srinivasan KK, Krishnan SR. Comparison of propane and methane performance and emissions in a turbocharged direct injection dual fuel engine. Trans ASME: J Eng Gas Turb Power 2011;133(9):092806. http://dx.doi.org/10.1115/1.4002895. 9p.
[32] Liu Z, Karim GA. The ignition delay period in dual fuel engines. SAE paper 950466; 1995.
[33] Heywood JB. Internal combustion engine fundamentals. McGraw-Hill, Inc.; 1988.
[34] Hohenberg G. Advanced approaches for heat transfer correlations. SAE paper 790825; 1979.
[35] Flynn PF, Durrett RP, Hunter GL, zur Loye AO, Akinyemi OC, Dec JE et al. Diesel combustion: an integrated view combining laser diagnostics, chemical kinetics, and empirical validation. SAE paper 1999-01-0509; 1999.
[36] Akihama K, Takatori Y, Inagaki K, Sasaki S, Dean AM. Mechanism of the smokeless rich diesel combustion by reducing temperature. SAE paper 2001-01-0655; 2001.
[37] Law CK. Combustion physics. Cambridge University Press; 2010.
[38] Glassman I, Yetter RA. Combustion. 4th ed. Academic Press; 2008.
[39] Karim GA. An examination of some measures for improving the performance of gas fuelled diesel engines at light load. SAE paper 912366; 1991.